Physical modeling of simultaneous heat and mass transfer: species interdiffusion, Soret effect and Dufour effect

Nan Jiang, Etienne Studer, Bã©rengã¨re Podvin

Version of Record: https://www.sciencedirect.com/science/article/pii/S0017931019364725
Manuscript_16b6ba9c784c28a9822b299a148331cc

Physical Modeling of Simultaneous Heat and Mass Transfer: Species Interdiffusion, Soret effect and Dufour effect

Nan Jiang[a,b,*], Etienne Studer[a], Bérengère Podvin[b]

[a] *DEN/STMF, CEA, Université Paris-Saclay, F-91191 Gif-sur-Yvette Cedex, France*
[b] *LIMSI, CNRS, Université Paris-Saclay, Bât 508, rue John von Neumann, Campus Universitaire, F-91405 Orsay, France*

Abstract

In problems involving simultaneous heat and mass transfer there exist coupling between these phenomena: temperature gradient may cause mass flux (Soret effect) and concentration gradient may cause heat flux (species interdiffusion and Dufour effect). In a large number of scientific works the authors do not include these effects into their models, without providing any justifications. In this paper we model natural convection inside a two-dimensional square cavity having evaporation and condensation boundary conditions. All coupling effects are taken into account and their relative impacts on numerical solutions are accurately assessed. Numerical results demonstrate that the species interdiffusion phenomenon has to be taken into account in order to guarantee the energy conservation in the domain. The influence of Soret and Dufour effects is examined and it is shown that for a binary mixture of steam and air these two effects have negligible contribution. We point out, however, that for some circumstances involving large thermal diffusion ratios Dufour effect may become important.

Keywords: natural convection, evaporation, condensation, square cavity, species interdiffusion, Soret and Dufour effects

1. Introduction

During some postulated accidents inside a nuclear reactor building, a large amount of hot water vapor can be released inside the containment. The steam condensation at the walls and structures of the reactor building has a mitigation effect in pressure rise inside in the containment. In order to assess this effect, one has to have a reliable physical model in which heat and mass transfer phenomena, including coupling between them, are extensively validated. In a large number of scientific works the authors do not include the coupling effects into their models, without providing any justifications. However, these can be very important inside boundary layers where large temperature and concentration gradients are present. This paper represents a first step of the validation work where we consider a comprehensive physical model involving all coupling effects. For the sake of simplicity, we test our model using a two-dimensional square cavity depicted on the Figure 1a.

At the left wall of the cavity, called in what follows, the hot wall, water evaporation takes place at a constant temperature T_H. A constant concentration of water vapor Y_v

*Corresponding author
Email address: nan.jiang@cea.fr (Nan Jiang)

is taken at saturation condition at temperature T_H. At the right wall, further called the cold wall, water condensation occurs at constant temperature T_C. The value for the mass fraction of vapor $Y_{v,C}$ is determined, as before, at saturation condition at T_C. The boundary values at the hot (resp. cold) wall will be denoted in this paper with a subscript $\bullet_H$ (resp. $\bullet_C$).

Double diffusion model for temperature and concentration, which has been widely applied to this problem [1, 2], neglect species interdiffusion, Soret effect and Dufour effect. Sun et al. [2] applied the low Mach number model to a similar problem and the effect of the total pressure variation was taken into account. The dimensionless form of their system of equations does not allow to consider a mixture of two gases having different specific heat ratios, which is an essential shortcoming. Moreover, the authors neglected the species interdiffusion phenomenon meaning that the model remains double-diffusive. In order to enforce the energy conservation inside the computational domain, the authors redefined the Nusselt number and Sherwood number according to the mathematical form of their energy transport equation. This modification enables them to balance the total Nusselt numbers on the left and right sides of the cavity at the steady state at the cost of losing the physical meaning of these numbers.

Weaver and Viskanta [3] investigated the influence of species interdiffusion under small heat capacity variation, alongside with Soret and Dufour effects. But the formulation of their Dufour effect heat flux is not consistent and more development is needed. A simplified model, as recently applied by Kefayati [4, 5, 6], takes into account these effects. The study is carried out in a similar square cavity without condensation or evaporation.

The aim of our paper is to propose a low-Mach number model which satisfies the energy conservation law which will be confirmed by the balance of total Nusselt numbers on both sides of the cavity. The definition of the total Nusselt number involve all coupling effects in accordance to the solved equations. Moreover, the model allows having different specific heat ratios for each component of the binary mixture. The paper is organized as follows. Section 2 describes the physical phenomena that we consider. Section 3 introduces the nondimensionalization. Section 4 describes our algorithm. Section 5 compares the current results to the litterature. Section 6 presents the computed results for air-steam mixture.

2. Analysis

We denote in the following ρ the density, P the pressure, T the temperature, Y_i the mass fraction of a component c_p (c_v respectively) the specific heat at constant pressure (at constant volume respectively), h the specific enthalpy, $\boldsymbol{U}$ the velocity, $\boldsymbol{\phi}$ the mass flux, $\boldsymbol{g}$ the gravitational acceleration and m the total mass of gas in the cavity. An indexed physical quantity s_i means the partial quantity s of component $i \in \{a, v\}$.The binary mass diffusion coefficient D and the kinetic viscosity ν are supposed to be constant. The gas mixture satisfies the Navier-Stokes equations as follows [7]:

$$\frac{\partial \rho}{\partial t} + \nabla \cdot \rho \boldsymbol{U} = 0, \tag{1}$$

$$\frac{\partial \rho Y_i}{\partial t} + \nabla \cdot \rho Y_i \boldsymbol{U} = -\nabla \cdot \boldsymbol{j}_i, \tag{2}$$

$$\frac{\partial \rho \boldsymbol{U}}{\partial t} + \nabla \cdot \rho \boldsymbol{U} \otimes \boldsymbol{U} = -\nabla P + \nabla \cdot \boldsymbol{\tau} + \rho \boldsymbol{g}, \tag{3}$$

$$\frac{\partial \rho \left(h + \frac{1}{2}\|\boldsymbol{U}\|^2\right)}{\partial t} + \nabla \cdot \rho \boldsymbol{U} \left(h + \frac{1}{2}\|\boldsymbol{U}\|^2\right) = -\nabla \cdot (\boldsymbol{q} + \boldsymbol{U} \cdot \boldsymbol{\tau}) + \frac{\partial P}{\partial t}, \tag{4}$$

Nomenclature

Greek Symbols

α_d	thermal diffusion ratio
$\boldsymbol{\phi}$	mass flux
$\boldsymbol{\tau}$	stress tensor
$\Delta\bullet$	difference between two wall values, $\cdot_H - \cdot_C$
γ	specific heat ratio
ν	kinetic viscosity
ρ	density
ε_m	mass non-Boussinesq factor, $\Delta r / r_{\text{ref}}$
ε_t	thermal non-Boussinesq factor, $\Delta T / T_{\text{ref}}$

Dimensionless Numbers

Fr	Froude number, $U_{\text{ref}}/\sqrt{gL}$
Nu	Nusselt number
Pr	Prandtl number, $\rho_{\text{ref}} c_{p,\text{ref}} \nu / k$
Ra	Rayleigh number, $\frac{\rho_{\text{ref}} c_{p,\text{ref}} g L^3 (\varepsilon_t + \varepsilon_m)}{\nu k}$
Re	Reynolds number, $U_{\text{ref}} L / \nu$
Sc	Schmidt number, ν / D
Sh	Sherwood number

Roman Symbols

$\boldsymbol{g}$	gravitational acceleration
$\boldsymbol{j}$	mass flux
$\boldsymbol{q}$	energy flux
$\boldsymbol{U}$	velocity
c_p	specific heat capacity at constant pressure
c_v	specific heat capacity at constant volume
D	binary mass diffusion coefficient
h	specific enthalpy
k	thermal conductivity
M	molar mass
m	total mass of the gas in the cavity
P	pressure
P_{th}	thermodynamic pressure
p_d	dynamic pressure
R	gas constant
r	specific gas constant of mixture
T	temperature
t	time
Y	mass fraction

Superscripts

$\bullet^\star$	corresponding dimensionless quantity

Subscripts

$\bullet_{\text{ref}}$	reference value for nondimensionalization
$\bullet_a$	advection
$\bullet_C$	value of a quantity on the cold wall
$\bullet_D$	Dufour effect
$\bullet_d$	diffusion
$\bullet_H$	value of a quantity on the hot wall
$\bullet_I$	species interdiffusion
$\bullet_i$	component i, where $i = a$ for air and $i = v$ for steam
$\bullet_S$	Soret effect

where $\boldsymbol{j}_i = \boldsymbol{j}_{i,d} + \boldsymbol{j}_{i,S}$ and $\boldsymbol{q} = \boldsymbol{q}_d + \boldsymbol{q}_I + \boldsymbol{q}_D$. We apply Fick's law $\boldsymbol{j}_{i,d} = -\rho D \nabla Y_i$ and Fourier's law $\boldsymbol{q}_d = -k \nabla T$ following [8]. In addition, (1) and (2) lead to $\sum_i \boldsymbol{j}_i = \boldsymbol{0}$. From (2), one identifies the partial mass flux of i-th component $\boldsymbol{\phi}_i = Y_i \boldsymbol{\phi} + \boldsymbol{j}_i$ and one defines the i-th component partial velocity as $\boldsymbol{U}_i = \boldsymbol{U} + \frac{\boldsymbol{j}_i}{\rho Y_i}$.

2.1. Gas properties

All the definitions in the following section can be found in [8]. We consider the ideal gas model for the gas mixture. To simplify the work, we consider a binary mixture consists of two gases with the following propertiees: the two gases obey separately the ideal gas law $\rho_i = \frac{P_i}{r_i T}$ where we define $r_i = R/M_i$ the specific gas constant; for each gas, the specific heat ratio $\gamma_i = c_{p,i}/c_{v,i}$ is constant; the internal energy of the mixture is equal to the sum of the partial internal energies: $\rho e = \sum_i \rho_i e_i$. These assumptions lead to the following properties of the binary gas mixture: $c_{p,i}$ and $c_{v,i}$ are constant; the mixture satisfies the ideal gas law $\rho = \frac{P}{rT}$; the enthalpy of the mixture is equal to the sum of the partial enthalpies: $\rho h = \sum_i \rho_i h_i$; the specific gas constant r and the specific heats of the mixture c_v and c_p are independent of temperature and equal to the weighted average of the each substance weighted by their mass fraction: $s = \sum_i Y_i s_i$ where $s = r, c_v$ or c_p; the specific heat ratio γ is independent of temperature and function only of the composition; the Mayer's relation holds: $r = c_p - c_v$.

2.2. Species interdiffusion

The enthalpy per unit volume of the mixture is the sum of partial enthalpies per unit volume of each component: $\sum_i \rho Y_i h_i = \rho h$. However, the enthalpy flux per unit volume is not equal to the sum of partial fluxes per unit volume, i.e. $\sum_i \rho_i h_i \boldsymbol{U}_i = \sum_i h_i (\rho_i \boldsymbol{U} + \boldsymbol{j}_i) = \rho h \boldsymbol{U} + \sum_i h_i \boldsymbol{j}_i$. The term $\sum_i h_i \boldsymbol{j}_i$ shows that there exists a heat flux induced by the concentration transport, which we call species interdiffusion flux or simply the interdiffusion flux, noted $\boldsymbol{q}_I = \sum_i h_i \boldsymbol{j}_i$. Note that the interdiffusion flux is independent of the transport of specific heat induced by the transport of concentration. In the case of a binary mixture, the expression yields to $\boldsymbol{q}_I = (c_{p,v} - c_{p,a})\, T \boldsymbol{j}_v$.

2.3. Soret and Dufour effects

According to [8], Soret and Dufour effects appear in the case of simultaneous mass and heat transfer as a result of chemical potential. We shall use expressions [8]: $\boldsymbol{j}_{v,S} = \alpha_d \rho D Y_v (1 - Y_v) \frac{1}{T} \nabla T$ and $\boldsymbol{q}_D = \alpha_d R T \frac{M}{M_a M_v} \boldsymbol{j}_v$ where α_d is the thermal diffusion ratio for vapour in air. Note that $\boldsymbol{j}_v = \boldsymbol{j}_{v,d} + \boldsymbol{j}_{v,S}$ and that $\boldsymbol{q}_I$ and $\boldsymbol{q}_D$ depend both on $\boldsymbol{j}_v$. We define respectively the interdiffusion heat flux and the Dufour effect heat flux originated from Fick's law mass flux and Soret effect mass flux, noted as $\boldsymbol{q}_{Id}$, $\boldsymbol{q}_{IS}$, $\boldsymbol{q}_{Dd}$ and $\boldsymbol{q}_{DS}$.

2.4. Velocity boundary conditions modelling wall condensation and evaporation

In the case of binary mixture of air and steam, one obtains by noticing $Y_a = 1 - Y_v$ and $\boldsymbol{j}_v = -\boldsymbol{j}_a$, $\boldsymbol{U}_a = \boldsymbol{U} - \frac{1}{\rho(1-Y_v)} \boldsymbol{j}_v$. On the vertical walls, because air is incondensable, the air mass flux through the boundary is zero, i.e. $U_{a,n} = 0$. This leads to $U|_{\text{wall},n} = \frac{j_{v,n}}{\rho(1-Y_v)}$ on these walls. When Soret effect is neglected, the mass flux is only constituted by Fick's law mass flux and the boundary condition becomes $U|_{\text{wall},n} = -\frac{D}{(1-Y_v)} \frac{\partial Y_v}{\partial n}$ which is called Stefan's velocity.

3. Scaling analysis

3.1. Nondimensionalization

In the square cavity problem, we have $Y_{v,H}$ and $Y_{v,C}$ as the highest and lowest steam mass fractions, and we define $Y_{v,\text{ref}} = \frac{1}{2}(Y_{v,H} + Y_{v,C})$, $\Delta Y_v = Y_{v,H} - Y_{v,C}$ and dimensionless

parameter $Y^\star$ varying from -0.5 to $+0.5$: $Y_v = Y_{v,\mathrm{ref}} + \Delta Y_v Y^\star$. Similarly, we set $T = T_{\mathrm{ref}} + \Delta T T^\star$, where T is the dimensionless temperature varying from -0.5 to $+0.5$. The reference state defining ρ_{ref}, r_{ref} and $c_{p,\mathrm{ref}}$ with subscript ref of the gas is taken at the initial pressure $P_{\mathrm{th,ref}}$ and at T_{ref} and $Y_{v,\mathrm{ref}}$. We define the following dimensionless numbers: Rayleigh number $\mathrm{Ra} = \frac{\rho_{\mathrm{ref}} c_{p,\mathrm{ref}} g L^3 (\varepsilon_t + \varepsilon_m)}{\nu k}$, Prandtl number $\mathrm{Pr} = \rho_{\mathrm{ref}} c_{p,\mathrm{ref}} \nu / k$, Schmidt number $\mathrm{Sc} = \nu / D$, Reynolds number $\mathrm{Re} = U_{\mathrm{ref}} L / \nu$, Froude number $\mathrm{Fr} = U_{\mathrm{ref}} / \sqrt{gL}$. Here we take $U_{\mathrm{ref}} = \sqrt{gL(\varepsilon_t + \varepsilon_m)}$, thus $\mathrm{Re} = \sqrt{\mathrm{Ra}/\mathrm{Pr}}$. The non-Boussinesq factors are introduced: $\varepsilon_t = \Delta T / T_{\mathrm{ref}}$ and $\varepsilon_m = \Delta r / r_{\mathrm{ref}}$, where $\Delta r = r_H - r_C$.

3.2. Low Mach number model

The low Mach number model is based on the acoustic wave filtering introduced by Paolucci. [9]. The idea is, with a low Mach number of the flow, to separate the pressure into a thermodynamic pressure P_{th} and a dynamic one p_d. The calculation of the thermodynamic pressure is based on the total mass conservation in the volume, and it can be calculated by $P_{\mathrm{th}} = m \left(\int_\Omega \frac{1}{rT} \mathrm{d}V \right)^{-1}$. Furthermore, the assumption of low Mach number enables us to neglect the dissipation of kinetic energy by viscous force and the spatial variation of pressure [9].

By defining $\boldsymbol{\phi} = \rho \boldsymbol{U}$, we write the non-dimensional low Mach number model for (1, 2, 3, 4) as :

$$\frac{\partial}{\partial t^\star} \rho^\star + \nabla^\star \cdot \boldsymbol{\phi}^\star = 0 \tag{5}$$

$$\frac{\partial}{\partial t^\star} \left(\rho^\star \boldsymbol{U}^\star \right) + \nabla^\star \cdot \left(\boldsymbol{\phi}^\star \otimes \boldsymbol{U}^\star \right) = \nabla^\star \cdot \boldsymbol{\tau}^\star + \frac{\rho^\star - 1}{\varepsilon_t + \varepsilon_m} \frac{\boldsymbol{g}}{\|g\|} - \nabla^\star p_d^\star \tag{6}$$

$$\frac{\partial}{\partial t^\star} \left(\rho^\star c_p^\star T^\star \right) + \nabla^\star \cdot \left(\boldsymbol{\phi}^\star c_p^\star T^\star \right) = \frac{\gamma - 1}{\gamma \varepsilon_t} \frac{\mathrm{d}P_{\mathrm{th}}^\star}{\mathrm{d}t^\star} - \frac{1}{\mathrm{Re}\,\mathrm{Pr}} \nabla^\star \left(\boldsymbol{q}_d^\star + \boldsymbol{q}_{Id}^\star + \boldsymbol{q}_{IS}^\star + \boldsymbol{q}_{Dd}^\star + \boldsymbol{q}_{DS}^\star \right) \tag{7}$$

$$\frac{\partial}{\partial t^\star} \left(\rho^\star Y^\star \right) + \nabla^\star \cdot \left(\boldsymbol{\phi}^\star Y^\star \right) = -\frac{1}{\mathrm{Re}\,\mathrm{Sc}} \nabla^\star \cdot \left(\boldsymbol{j}_{v,d}^\star + \boldsymbol{j}_{v,S}^\star \right) \tag{8}$$

where $\boldsymbol{\tau}$ is the viscosity stress tensor: $\boldsymbol{\tau}^\star \left(\boldsymbol{U}^\star \right) = \frac{1}{\mathrm{Re}} \left(\nabla^\star \boldsymbol{U}^\star + \left(\nabla^\star \boldsymbol{U}^\star \right)^T \right) - \frac{2}{3} \frac{1}{\mathrm{Re}} \nabla^\star \cdot \boldsymbol{U}^\star \boldsymbol{I}$ and the thermodynamic pressure is $P_{\mathrm{th}}^\star = m^\star \left(\int_\Omega (1 + \varepsilon_t T^\star)^{-1} (1 + \varepsilon_m Y^\star)^{-1} \mathrm{d}V \right)^{-1}$. Using the result from Section 2.4, the boundary conditions are the following:

- on the horizontal walls, $U_x^\star = U_y^\star = 0$ and $\frac{\partial T^\star}{\partial n} = 0$, $\frac{\partial Y^\star}{\partial n} = 0$.
- on the cold (resp. hot) wall, $T^\star = Y^\star = -0.5$, (resp., $T^\star = Y^\star = +0.5$).
- on the hot and cold walls, $U_y^\star = 0$ and $U_x^\star = U_{\mathrm{wall},n}^\star = \frac{\Delta Y_v}{1 - Y_v} \frac{1}{\mathrm{Re}\,\mathrm{Sc}} \frac{1}{\rho^\star} \left(\boldsymbol{j}_{v,d}^\star + \boldsymbol{j}_{v,S}^\star \right) \cdot \boldsymbol{e}_x$.

3.3. Definition of Nusselt and Sherwood number

The Nusselt number consists, like the heat flux itself, of 6 parts: Nu_a due to advection, Nu_d due to diffusion, $\mathrm{Nu}_I = \mathrm{Nu}_{Id} + \mathrm{Nu}_{IS}$ due to interdiffusion (where Nu_{Id} is related to diffusive mass flux and Nu_{IS} is related to Soret effect mass flux) and $\mathrm{Nu}_D = \mathrm{Nu}_{Dd} + \mathrm{Nu}_{DS}$ due to Dufour effect (where Nu_{Dd} related to mass flux and Nu_{DS} related to Soret effect mass flux). Hence, one may find the expression of the dimensionless heat flux as following: $\boldsymbol{q}_a^\star = \mathrm{Re}\,\mathrm{Pr}\, \rho^\star c_p^\star \left(\frac{1}{\varepsilon_t} + T^\star \right) \boldsymbol{U}^\star$, $\boldsymbol{q}_d^\star = -\nabla^\star T^\star$, $\boldsymbol{q}_{Id}^\star = -\frac{\mathrm{Pr}}{\mathrm{Sc}} \frac{\Delta c_p}{c_{p,\mathrm{ref}}} \left(\frac{1}{\varepsilon_t} + T^\star \right) \rho^\star \nabla^\star Y^\star$, $\boldsymbol{q}_{IS}^\star =$

$-\frac{\mathrm{Pr}}{\mathrm{Sc}}\frac{\Delta c_p}{c_{p,\mathrm{ref}}}\frac{Y_v(1-Y_v)}{Y_{v,H}-Y_{v,C}}\alpha_d\rho^\star\nabla^\star T^\star$, $\boldsymbol{q}^\star_{Dd} = -\frac{\mathrm{Pr}}{\mathrm{Sc}}\frac{\alpha_d R^2}{rc_{p,\mathrm{ref}}M_aM_v}\left(\frac{1}{\varepsilon_t}+T^\star\right)\rho^\star\nabla^\star Y^\star$,
$\boldsymbol{q}^\star_{DS} = -\frac{\mathrm{Pr}}{\mathrm{Sc}}\frac{\alpha_d^2 R^2}{rc_{p,\mathrm{ref}}M_aM_v}\frac{Y_v(1-Y_v)}{Y_{v,H}-Y_{v,C}}\rho^\star\nabla^\star T^\star$. In the same way, the different contributions to the mass flux, due to advection, diffusion and Soret effect, are identified as following: $\boldsymbol{j}^\star_{v,a} = \mathrm{Re}\,\mathrm{Sc}\,\rho^\star\left(\frac{Y_{v,\mathrm{ref}}}{Y_{v,H}-Y_{v,C}}+Y^\star\right)\boldsymbol{U}^\star$, $\boldsymbol{j}^\star_{v,d} = -\rho^\star\nabla^\star Y^\star$, $\boldsymbol{j}^\star_{v,S} = -\alpha_d\rho^\star\frac{Y_v(1-Y_v)}{Y_{v,H}-Y_{v,C}}\frac{\varepsilon_t}{1+\varepsilon_t T^\star}\nabla^\star T^\star$.
In the following sections, these average values of Nusselt and Sherwood numbers are going to be computed along either cold or hot wall by the following: $\overline{\mathrm{Nu}_\bullet} = \int_{\mathrm{wall}}\boldsymbol{q}^\star_\bullet\cdot\boldsymbol{e}_n$, $\overline{\mathrm{Sh}_\bullet} = \int_{\mathrm{wall}}\boldsymbol{j}^\star_{v,\bullet}\cdot\boldsymbol{e}_n$, where $\boldsymbol{e}_n$ is the normal vector to the surface.

4. Numerical solution

The solution of the original system demands non-zero velocity boundary conditions given by Stefan's velocity calculated from the vapour distribution at current time step. However, this definition of boundary condition may cause instability of the algorithm. Our solution to this problem is to build a decomposition of $\boldsymbol{U}$ as $\boldsymbol{U}_{\mathrm{int}}+\boldsymbol{U}_b$, where $\boldsymbol{U}_{\mathrm{int}}=0$ on each wall (no matter if there is a phase change or not) and $\boldsymbol{U}_b$ is a partial velocity indicating the boundary condition of $\boldsymbol{U}$.

4.1. Definition of a boundary condition of velocity

For the case of a square cavity, there exists actually two types of walls with or without phase changes in our physical scenario. In the case of an adiabatic and impermeable wall, the boundary condition is $\boldsymbol{U}=0$. The condition for $\boldsymbol{U}_b$ is therefore $\boldsymbol{U}_b=0$. In the case of a wall with evaporation or condensation, the tangential velocity $U_t=0$ and the normal velocity $U_n=\rho^{-1}(1-Y_v)^{-1}\boldsymbol{j}_v\cdot\boldsymbol{e}_n$ therefore $\boldsymbol{U}_b=(\rho^{-1}(1-Y_v)^{-1}\boldsymbol{j}_v\cdot\boldsymbol{e}_n)\boldsymbol{e}_n$. The idea is to define a phase-change factor f_k associated with each wall k such that $\boldsymbol{U}_b=-\sum_k f_k(\rho^{-1}(1-Y_v)^{-1}\boldsymbol{j}_v\cdot\boldsymbol{e}_{n,k})\boldsymbol{e}_{n,k}$. On each wall k, f_k is either equal to 1 if phase change is present or 0 otherwise.

Now we need to search for the value of f_k inside the domain. The simplest possible definition, which consists in taking $f_k=0$ in the interior of the domain, is actually equivalent to the Stefan's-velocity-type boundary condition and causes the discontinuity of U_b . We need a more "smooth" definition of f_k. In order to keep the continuity of $\boldsymbol{U}_b$, one may assume $\nabla^2 f_k=0$. In practice, we solve the factors f_k at the initialization step of the algorithm. The dimensionless air diffusive velocity is calculated by $\boldsymbol{U}^\star_{a,d}=\frac{1}{\mathrm{Re}\,\mathrm{Sc}}\frac{Y_{v,H}-Y_{v,C}}{1-Y_v}\left(\nabla^\star Y^\star+\alpha_d\frac{Y_v(1-Y_v)}{Y_{v,H}-Y_{v,C}}\frac{\varepsilon_T}{1+\varepsilon_T T^\star}\nabla^\star T^\star\right)$. Finally, in the low Mach model, the equation (6) is replaced by

$$\begin{aligned}\frac{\partial}{\partial t^\star}(\rho^\star\boldsymbol{U}^\star_{\mathrm{int}})+\nabla^\star\cdot(\boldsymbol{\phi}^\star\boldsymbol{U}^\star_{\mathrm{int}}) \;=\; &\nabla^\star\cdot\boldsymbol{\tau}^\star(\boldsymbol{U}^\star_{\mathrm{int}})+\frac{\rho^\star-1}{\varepsilon_T+\varepsilon_m}\frac{\boldsymbol{g}}{\|g\|}-\nabla^\star p^\star_d\\ &-\left(\frac{\partial}{\partial t^\star}(\rho^\star\boldsymbol{U}^\star_b)+\nabla^\star\cdot(\boldsymbol{\phi}^\star\boldsymbol{U}^\star_b)-\nabla^\star\cdot\boldsymbol{\tau}^\star(\boldsymbol{U}^\star_b)\right)\end{aligned}\tag{9}$$

and the whole system of (5), (9), (7) and (8) is subject to the boundary conditions in 3.2 and $U^\star_{\mathrm{int}}=0$ when $x^\star=0,1$ or $y^\star=0,1$. For the computation of $\boldsymbol{U}^\star_{\mathrm{int}}$ and $p^\star_d$, we apply the Pressure Implicit Splitting of Operators (PISO) algorithm based on OpenFOAM framework.

4.2. Adjustment of thermodynamic pressure

Mass conservation needs to be enforced through the Poisson equation. In an incompressible system, the only way to keep the mass conservation is to balance the inlet and outlet of mass. However, in a low Mach system, we gain the possibility to adjust the mass in a constant volume by raising the density of the fluid. The way that we implement this idea is to adjust the thermodynamic pressure P_{th}. In order to adjust P_{th} we calculate first the mass flux $\frac{\mathrm{d}m}{\mathrm{d}t} = \int_\Omega \nabla \cdot \boldsymbol{\phi} \mathrm{d}V$ and thus at time $t + \Delta t$: $P^\star_{\mathrm{th}}(t^\star + \Delta t^\star) = \frac{m^\star(t^\star) + \frac{\mathrm{d}m^\star}{\mathrm{d}t^\star}\Delta t^\star}{\int_{\Omega^\star} \frac{1}{(1+\varepsilon_T T^\star)(1+\varepsilon_m Y^\star)} \mathrm{d}V^\star}$ This updated value $P^\star_{\mathrm{th}}(t + \Delta t)$ is used to calculate the physical parameters in the following iterations within the time step. Once the internal iteration is finished, we enforce the total air mass unchanged by updating $m(t^\star + \Delta t^\star) = \frac{m^\star_a \int_{\Omega^\star} \frac{1}{(1+\varepsilon_T T^\star)(1+\varepsilon_m Y^\star)} \mathrm{d}V^\star}{\int_{\Omega^\star} \frac{1-Y_{v,0}-\Delta Y_v Y^\star}{(1+\varepsilon_T T^\star)(1+\varepsilon_m Y^\star)} \mathrm{d}V^\star}$.

5. Validation and comparisons

Validation of our model was established [10] for purely thermal convection [11] as well as cases for the mixture with evaporation and condensation under nearly constant thermodynamic pressure [1]. The mesh convergence was obtained with a resolution of 160×160. All results in the present paper are computed using a mesh of 320×320.

The low Mach approximation is applied to the double-diffusive model in the work of Sun and Lauriat [2] in 2010. In their work, a case of large thermodynamic pressure variation is examined.

5.1. Case description

Since the dimensionless heat transport equation in the double-diffusive model can be transformed into conservative form, conservative heat fluxes may be reconstructed. In their paper [2], the definition of the Sherwood and Nusselt numbers are given by such reconstruction, which shall be translated in our notations as: $\mathrm{Sh} = \mathrm{Re}\,\mathrm{Sc}\,\rho^\star Y^\star \boldsymbol{U}^\star \cdot \boldsymbol{e}_n - \rho^\star \nabla^\star Y^\star \cdot \boldsymbol{e}_n$, $\mathrm{Nu} = \mathrm{Re}\,\mathrm{Pr}\,\rho^\star T^\star \boldsymbol{U}^\star \cdot \boldsymbol{e}_n - \rho^\star \nabla^\star T^\star \cdot \boldsymbol{e}_n$. It is clear that these definitions, which will be called the reconstructed definitions in the following to be differentiated from the physical definitions, do not take into account neither the reference mass fraction nor the reference temperature in advection and therefore are not equivalent to the physical definitions of advection Sherwood and Nusselt number. The transport properties of case 1 in Table 5 in [2] are shown in Table 1 (s1). In addition, in the initial conditions, the dimensionless temperature and concentration are set to be -0.5 in order to reinforce the evaporation and to increase the thermodynamic pressure variation. Since the amount of steam in the cavity is expected to increase from its initial value, the thermodynamic pressure is supposed to be bigger than 1. Table 1 compares results from the reference [2], results based on the double-diffusive approach using incorrect (reconstructed) definitions (ddR) and correct ones (dd), and results based on our full model.

5.2. Results

One notices that the reference result and the double diffusive result with reconstructed post-treatment are in very good agreement. This validates our low-Mach calculation without species interdiffusion. Comparison of specific contributions for the two double-diffusive cases, which are based on the same calculation, illustrates the difference in the definition of the Nusselt numbers. While the contributions to diffusion are the same, the

advective contributions are totally different. Since the reconstructed definitions do not take into account the reference values, it is possible to obtain negative values on the cold wall as the two dimensionless fields take negative values there. The double-diffusive case with the correct definition does not lead to matching Nusselt numbers on each side of the cavity.

In contrast, our calculation with our full model accounting for species interdiffusion leads to equal Nusselt numbers on each side. Since the specific heat capacity difference is large ($c_{p,v}/c_{p,a} = 4$), interdiffusion heat fluxes make a major contribution to the total heat transfer (46.50% of the total heat flux on the hot wall and 41.10% on the cold wall).

In conclusion, we have shown that the energy conservation is not guaranteed in double diffusive model.

6. Calculations for air and steam mixture

We investigate the influence of species interdiffusion together with Soret and Dufour effect for air steam mixture representative of our problem. We now consider a square cavity, side length of which is 2 cm, with an initial pressure of 5 bar. The Rayleigh number for this case is $\mathrm{Ra} = 4.05 \times 10^5$. We take $\mathrm{Pr} = 1.32$ and $\mathrm{Sc} = 0.66$. The temperature of the hot wall is $T_H = 120$ °C and that of the cold wall is $T_C = 80$ °C. Assuming the steam is saturated on both walls, we take $Y_{v,H} = 0.29$ and $Y_{v,C} = 0.06$. The initial state of the interior is set as the reference state.

6.1. Values of α_d

The intensity of Soret and Dufour effects is a function of the thermal diffusion ratio α_d, which depends on the composition of mixture, but is approximately independent to temperature and concentration of components [8]. When $\alpha_d = 0$, all the terms due to Soret and Dufour effects do not contribute. We therefore use this value to set up a reference result without Soret and Dufour effects, which is denoted as case e1 in Table 1. According to [12, 13], a realistic value $\alpha_d = -0.0059$ is found for the air-steam mixture and it is applied for the case e2. In [8], we find that α_d can reach 0.4 in a mixture of $\mathrm{Ne} - \mathrm{He}$ or $\mathrm{N_2} - \mathrm{H_2}$. This value is applied for the case e3 in order to assess to a maximal influence of Soret and Dufour effects. Consequently, we consider the following values of α_d in the calculations: 0 (e1), -0.0059 (e2), 0.4 (e3).

6.2. Results

First of all, according to comparison between the results of e1 and e2 (Table 1), the influence of Soret and Dufour effects remains slight with $\alpha_d = -0.0059$. The mass fluxes are mostly the same in the two cases and the Soret effect is negligible in the case e2. The heat fluxes are pratically not affected by the Dufour effect heat flux, which is negligible compared to the total heat flux. However, the Dufour effect shows a more important contribution to the total heat transfer (-0.31% / -0.42%) compared to that of Soret effect to the total mass transfer (-0.04% / -0.03%). In the case e3, Soret and Dufour effects are amplified. With their influence large difference in the case e1 is observed both in mass transfer and in heat transfer. Compared to e1, e3 shows that a positive α_d may intensify the mass transfer and the evaporation-condensation rate. It is also necessary to point out that in e3 the Dufour effect contributes significantly to the total heat transfer. However the Soret effect do not contribute a lot to the mass transfer even with a rather large α_d.

In Figure 1, (1c) and (1f) show the distribution of the temperature and the concentration fields in the cavity along the velocity streamlines. No visible difference is observed between cases e1 (1b and 1e) and e2 (1c and 1f), which agrees with the results in Table 1. Figures 1d and 1g show that the fluid is hotter and less rich in steam in the top portion while it is colder and richer in steam in the bottom portion. Moreover, the thermal boundary layers appear to be thicker on both vertical walls in Figure 1d, which is consistent with the reduced diffusion fluxes noted in Table 1. It is also observed that the velocity field is characterized by larger recirculation zones.

7. Conclusion

In this paper, we have presented a low Mach number model for the binary mixture of condensable and non-condensable gases with constant thermophysical properties. The model was applied to the case of a two-dimensional square cavity. A boundary condition treatment strategy based on the air partial velocity was implemented in the solver and was found to improve the robustness of the PISO algorithm.

Application of the model for different test cases showed that the contribution of interdiffusion to the Nusselt number was significant on both side walls of the cavity when $\Delta c_p/c_{p,\mathrm{ref}}$ is not negligible. Consideration of species interdiffusion is therefore essential to guarantee the energy conservation in the domain. It will be interesting to study the influence of $\Delta c_p/c_{p,\mathrm{ref}}$ on interdiffusion. Moreover, as species interdiffusion is not generally taken into account in study of turbulence, the inclusion of this phenomenon in the model and particularly in wall functions should be investigated.

The influence of Soret and Dufour effects was also examined. For a mixture of air and vapour, we established that these two effects are negligible. However, we found that Dufour effects may become important when the thermal diffusion ratio gets sufficiently large. This will bring us to reconsider the influence of Soret and Dufour effects if for example hydrogen or helium is involved.

References

[1] J. A. Weaver, R. Viskanta, Natural convection due to horizontal temperature and concentration gradients-1. Variable thermophysical property effects, International Journal of Heat and Mass Transfer 34 (12) (1991) 3107–3120.

[2] H. Sun, G. Lauriat, D. L. Sun, W. Q. Tao, Transient double-diffusive convection in an enclosure with large density variations, International Journal of Heat and Mass Transfer 53 (4) (2010) 615–625.

[3] J. A. Weaver, R. Viskanta, Natural convection due to horizontal temperature and concentration gradients-2. Species interdiffusion, Soret and Dufour effects, International Journal of Heat and Mass Transfer 34 (12) (1991) 3121–3133.

[4] G. R. Kefayati, FDLBM simulation of entropy generation in double diffusive natural convection of power-law fluids in an enclosure with Soret and Dufour effects, International Journal of Heat and Mass Transfer 89 (2015) 267–290.

[5] G. R. Kefayati, Simulation of double diffusive natural convection and entropy generation of power-law fluids in an inclined porous cavity with Soret and Dufour effects

(Part I: Study of fluid flow, heat and mass transfer), International Journal of Heat and Mass Transfer 94 (2016) 539–581.

[6] G. R. Kefayati, Simulation of double diffusive natural convection and entropy generation of power-law fluids in an inclined porous cavity with Soret and Dufour effects (Part II: Entropy generation), International Journal of Heat and Mass Transfer 94 (2016) 582–624.

[7] T. Poinsot, D. Veynante, Theoretical and Numerical Combustion, 2011.

[8] R. B. Bird, W. E. Stewart, E. N. Lightfoot, Transport Phenomena, 2nd Edition, John Wiley & Sons, Inc., 2001.

[9] S. Paolucci, On the filtering of sound from the Navier–Stokes equations, Tech. Rep. SAND82-8257, Sandia National Laboratoies, Livermore (1982).

[10] N. Jiang, E. Studer, B. Podvin, Improvement Of Physical Modeling For Coupled Heat And Mass Transfer In A Square Cavity With Condensation In The Presence Of Non-Condensable Gas, in: 18th International Topical Meeting on Nuclear Reactor Thermal Hydraulics (NURETH-18), Portland, OR, USA, 2019.

[11] H. Paillère, P. Le Quéré, C. Weisman, J. Vierendeels, E. Dick, M. Braack, F. Dabbene, A. Beccantini, E. Studer, T. Kloczko, C. Corre, V. Heuveline, M. Darbandi, S. F. Hosseinizadeh, Modelling of Natural Convection Flows with Large Temperature Differences: A Benchmark Problem for Low Mach Number Solvers. Part 2. Contributions to the June 2004 conference, ESAIM: Mathematical Modelling and Numerical Analysis 39 (3) (2005) 617–621.

[12] L. Monchick, E. A. Mason, Transport properties of polar gases, The Journal of Chemical Physics 35 (5) (1961) 1676–1697.

[13] E. A. Mason, Higher approximations for the transport properties of binary gas mixtures. I. general formulas, The Journal of Chemical Physics 27 (1) (1957) 75–84.

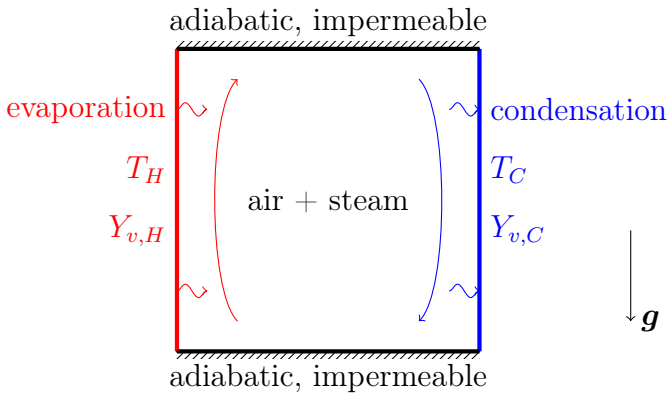

(a) Natural convection in binary gases with horizontal temperature and concentration gradients in a square cavity.

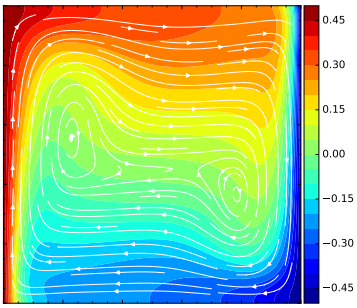

(b) $T^\star$ for e1

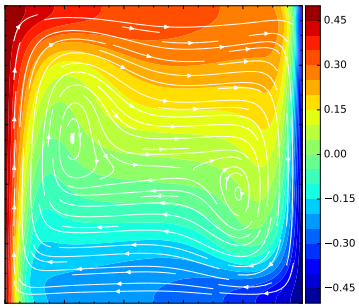

(c) $T^\star$ for e2

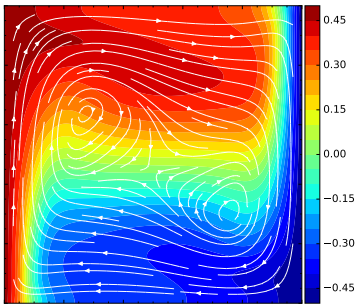

(d) $T^\star$ for e3

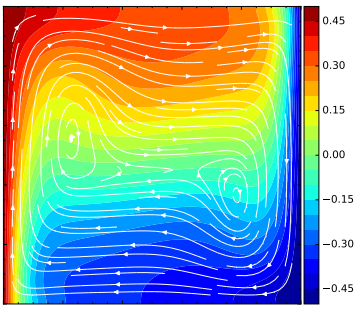

(e) $Y^\star$ for e1

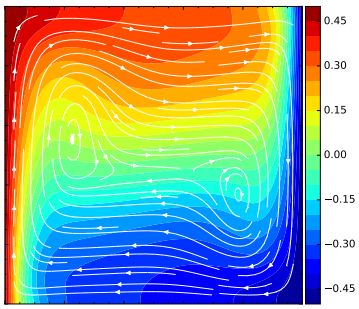

(f) $Y^\star$ for e2

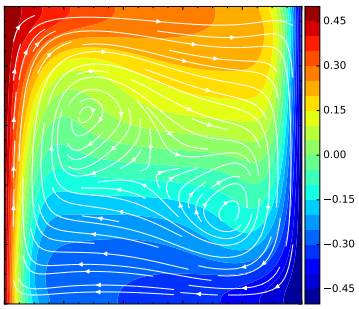

(g) $Y^\star$ for e3

Figure 1: Illustrations of dimensionless fields $T^\star$ and $Y^\star$ with the streamlines of velocity field of the calculation results of e2 and e3.

case	s1-ref	s1-ddR	s1-dd	s1-full	e1	e2	e3
Ra	5.63×10^6	5.63×10^6	5.63×10^6	5.63×10^6	4.05×10^5	4.05×10^5	4.05×10^5
Pr	0.71	0.71	0.71	0.71	1.32	1.32	1.32
Sc	0.71	0.71	0.71	0.71	0.66	0.66	0.66
M_a/g.mol^{-1}	29	29	29	29	29	29	29
M_v/g.mol^{-1}	7.25	7.25	7.25	7.25	18	18	18
γ_a	1.4	1.4	1.4	1.4	1.4	1.4	1.4
γ_v	1.4	1.4	1.4	1.4	1.29	1.29	1.29
T_H/K	352	352	352	352	393.15	393.15	393.15
T_C/K	288	288	288	288	353.15	353.15	353.15
$Y_{v,H}$	0.074	0.074	0.074	0.074	0.29	0.29	0.29
$Y_{v,C}$	0	0	0	0	0.06	0.06	0.06
α_d	—	—	—	0	0	-0.0059	0.4
model	ref.	ddR	dd	full	full	full	full
P^*_{th}	1.255	1.257	1.257	1.261	0.9988	0.9989	0.9915
				hot wall			
$\overline{\text{Sh}_a}$	—	0.71	1.42	1.41	1.85	1.85	2.05
$\overline{\text{Sh}_d}$	—	17.72	17.72	17.72	4.53	4.52	4.93
$\overline{\text{Sh}_S}$	—	—	—	0.00	0.00	0.00	0.08
$\overline{\text{Sh}}$	18.40	18.43	19.13	19.13	6.38	6.36	7.06
$\overline{\text{Nu}_a}$	—	0.78	8.56	8.56	31.65	31.57	35.04
$\overline{\text{Nu}_d}$	—	15.53	15.53	13.88	5.03	5.08	2.49
$\overline{\text{Nu}_{Id}}$	—	—	—	19.46	18.05	18.01	19.66
$\overline{\text{Nu}_{IS}}$	—	—	—	0.00	0.00	-0.01	0.32
$\overline{\text{Nu}_{Dd}}$	—	—	—	0.00	0.00	-0.17	12.80
$\overline{\text{Nu}_{DS}}$	—	—	—	0.00	0.00	0.00	0.21
$\overline{\text{Nu}}$	16.34	16.31	24.09	41.90	54.73	54.47	70.52
				cold wall			
$\overline{\text{Sh}_a}$	—	-0.71	0.00	0.00	0.39	0.39	0.43
$\overline{\text{Sh}_d}$	—	19.12	19.12	19.12	5.99	5.97	6.58
$\overline{\text{Sh}_S}$	—	—	—	0.00	0.00	0.00	0.05
$\overline{\text{Sh}}$	18.40	18.42	19.12	19.12	6.38	6.36	7.06
$\overline{\text{Nu}_a}$	—	-0.64	5.73	5.73	23.20	23.13	25.68
$\overline{\text{Nu}_d}$	—	16.93	16.93	18.93	10.07	10.17	3.55
$\overline{\text{Nu}_{Id}}$	—	—	—	17.20	21.45	21.40	23.59
$\overline{\text{Nu}_{IS}}$	—	—	—	0.00	0.00	-0.01	0.16
$\overline{\text{Nu}_{Dd}}$	—	—	—	0.00	0.00	-0.23	17.43
$\overline{\text{Nu}_{DS}}$	—	—	—	0.00	0.00	0.00	0.12
$\overline{\text{Nu}}$	16.34	16.30	22.67	41.86	54.72	54.46	70.53

Table 1: Input data and numerical results of different dimensionless numbers